CHAPTER 2

Migration of Common Midpoint Slant Stacks

2.1. Motivation

Migration with slant stacks of common midpoint gathers is a method which makes no assumptions which deteriorate with wide offset angles, steep dips, and vertical velocity variations. Events of different dips which intersect are equally well imaged. It permits the more accurate velocity analysis after migration when dipping reflections have been correctly located and diffraction noise removed. Refractions and post critical angle reflections which appear in slant stacks can also be used to estimate velocity.

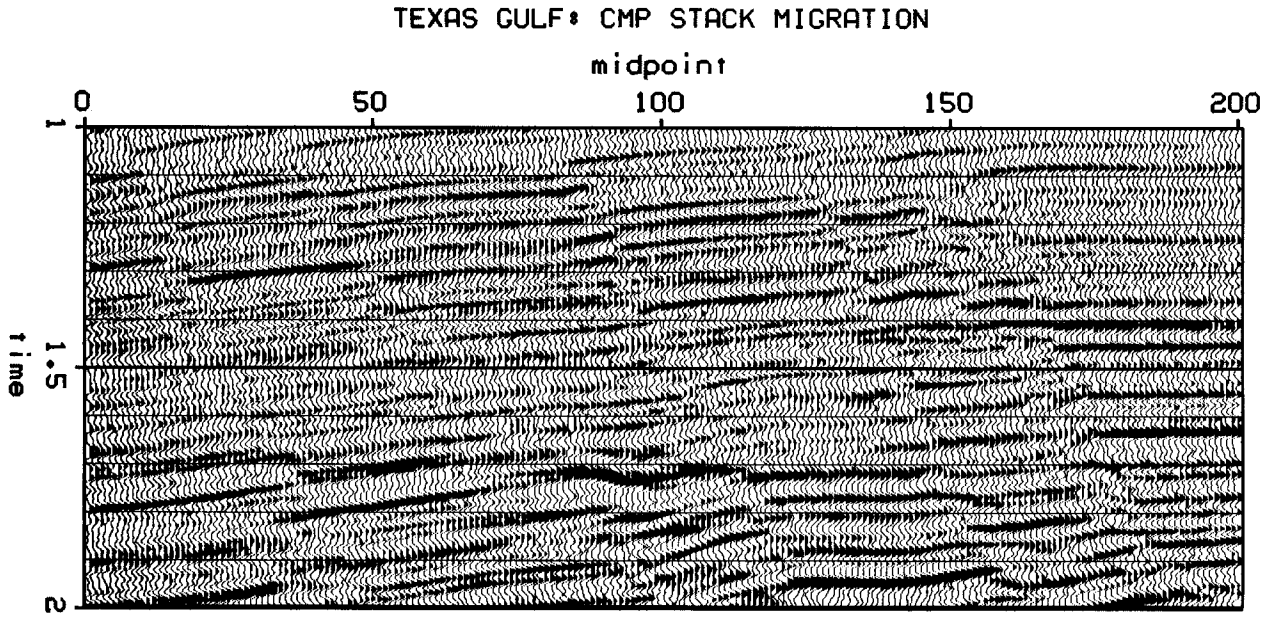

FIGURE 2.1: Conventional migration. CMP stack migration of a dataset from the Texas Gulf coast. The geology consists of several steep dipping growth faults.

Figure 2.1 shows the migration of a conventional stack of growth faults. Conventional common depth point stacking had obliterated the fault plane reflections present in the unstacked data as seen in Figure 2.2. Fortunately, slant stack migration recovers these fault plane reflections as shown in Figure 2.3.

2.2. Method of Migrating Common Midpoint Slant Stacks

There are three stages to migrating slant stacks. Mathematical details are given in the subsequent sections.

(1) First construct one or more slant stack sections. Figure 2.4 shows how a slant stack is done. Rather than sum along the hyperbolic trajectory of conventional stacking, a slant stack sums along inclined straight lines. A section is made of

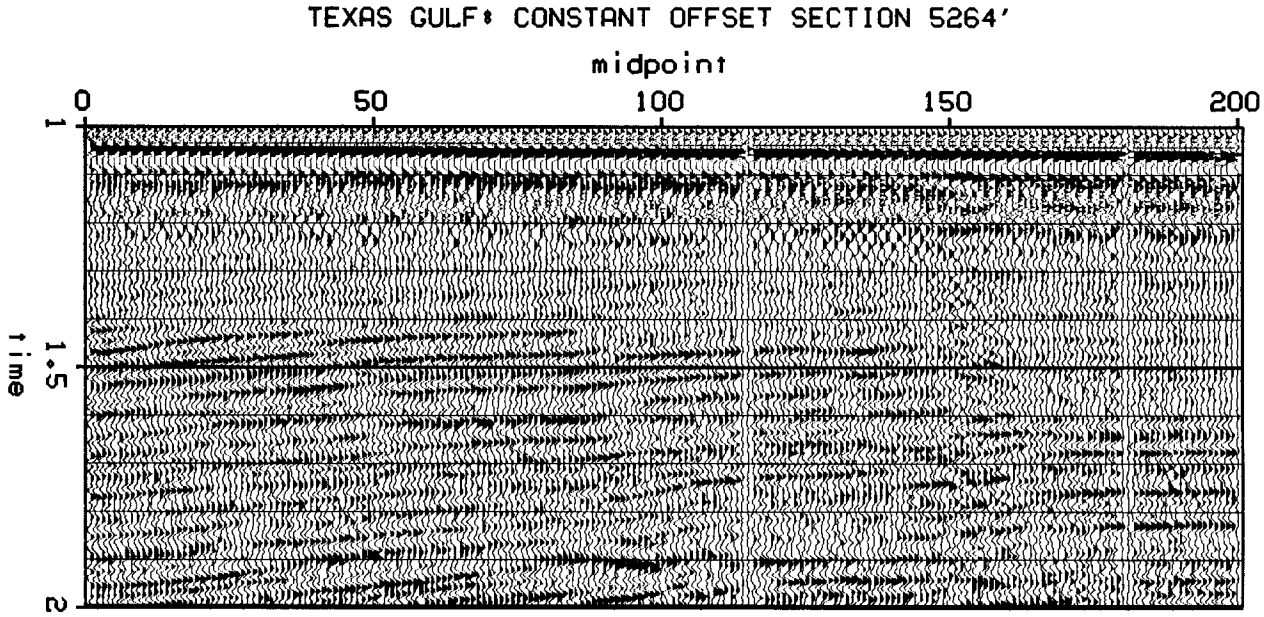

FIGURE 2.2: Constant offset section. A constant offset section from the same dataset as in Figure 2.1. Faint fault plane reflections are visible at this offset and most other offsets.

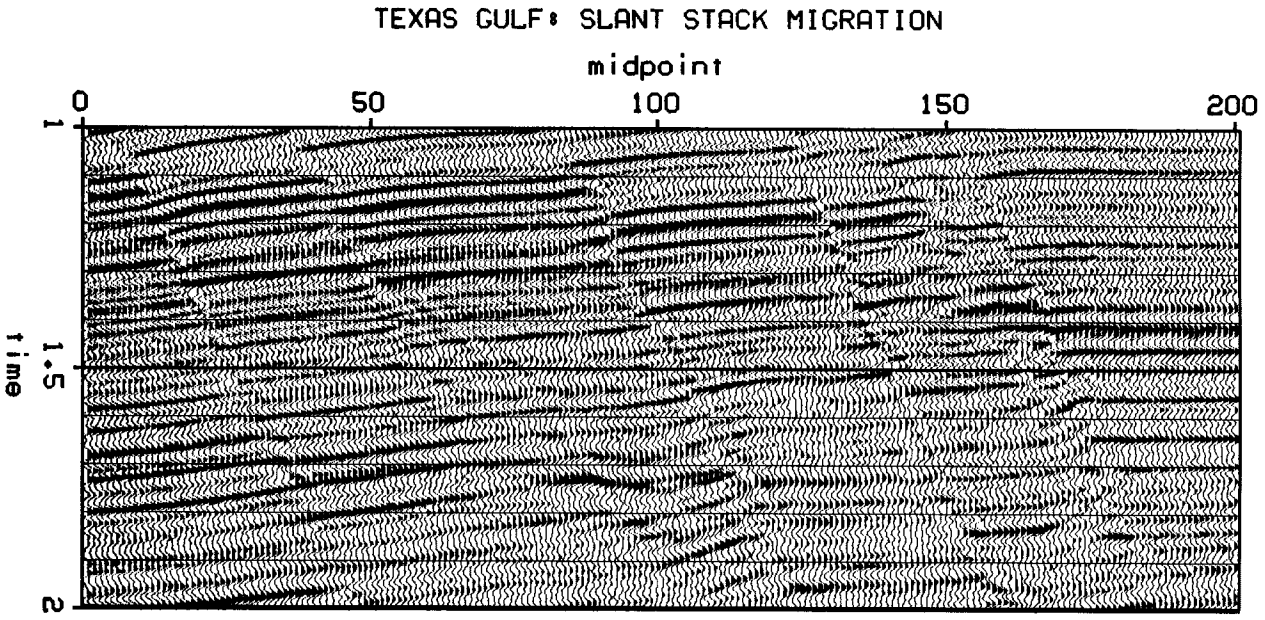

FIGURE 2.3: Slant stack migration. Midpoint slant stack migration of same dataset from Figure 2.1. Fault plane reflections are now visible. Lateral resolution is increased. For both the conventional stack and slant stack migrations, the same midpoints and direct arrival mutes were used. In both cases the migration equation was implemented using a phase shift algorithm in order to avoid inaccuracies in the migration implementation itself. The slant stack migration is a sum of the twenty different angle-midpoint sections shown in Figure 2.8.

the slant stack for a fixed slope from each common midpoint (CMP) gather.

(2) Second, migrate each of these sections.

(3) Finally, stack together one or more migrated sections. The main motivation is to improve the signal to noise in the result. A second reason is that a portion of the data may be absent on a slant stack made at one stacking slope, while present at another stacking slope.

2.3. Mathematical Description of Slant Stacking

A mathematical formulation shows how slant stacking relates to wave propagation. It lays the groundwork for deriving an equation for migrating slant

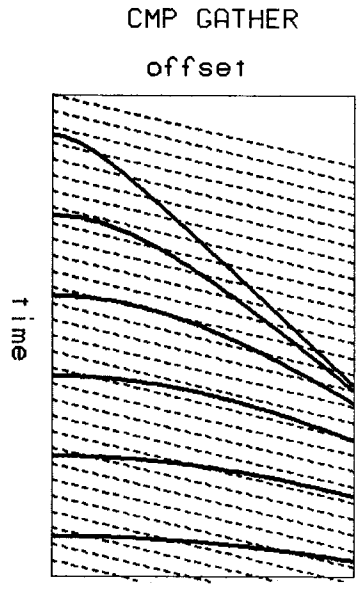

FIGURE 2.4: Process of slant stacking. A slant stack trace is formed by summing along an inclined linear trajectory across a CMP gather.

stacks.

Slant stacking may be thought of as a two step process. First, we apply a time shift to each trace of a CMP gather. The amount of the time shift is directly proportional to the offset. Second, we horizontally sum the time shifted traces across offset. This two step process is equivalent to summing along tilted linear trajectories across the gather.

Equation (2.1) is the coordinate transformation for the time shift.

$$h' = h \qquad t' = t - 2ph \tag{2.1}$$

where h is half offset, t is traveltime, and p is the slope of the time shift. (A factor of 2 here makes the migration equations look nice later.)

Next we find the frequency domain equivalent of equation (2.1). We first note that the seismic wavefield P is identical in either coordinate system.

$$P(h,t) = P(h',t') \tag{2.2}$$

Then we find the derivatives of one coordinate system in terms of the other.

$$\frac{\partial P'}{\partial t'} = \frac{\partial P}{\partial t} \qquad \frac{\partial P'}{\partial h'} = \frac{\partial P}{\partial h} + 2p\frac{\partial P}{\partial t} \tag{2.3}$$

In the frequency domain these relations are

$$\omega' = \omega \qquad k_h' = k_h + 2p\omega \tag{2.4}$$

where ω is the traveltime wavenumber and k_h the offset wavenumber.

The second step to slant stacking is to sum across offset. In the frequency domain this is equivalent to selecting the zeroth k_h' frequency.

$$0 = k_h + 2p\omega \tag{2.5}$$

In a slightly different form equation (2.5) is the well known frequency domain statement of Snell's law.

$$\boxed{\frac{k_h}{\omega} = -2p} \tag{2.6}$$

This equation says that slant stacking decomposes the CMP gather into portions with the same ray parameter p. We use the term ray parameter in the mathematical sense that it is the invariant in Snell's law and the time/offset slope of the data. However, the ray parameter concept does not represent raypaths or wavefronts in common midpoint coordinates. (In other words, one cannot design a field experiment to record a common midpoint slant stack.)

Equation (2.6) leads to a frequency domain method of slant stacking which is developed in appendix C.

2.4. Migration Equation for Common Midpoint Slant Stacks

Our imaging principle is that a sub-surface image of the earth is what would be recorded at zero traveltime if the seismic sources and receivers were located directly above the reflector. However, we are really recording traveltimes at the

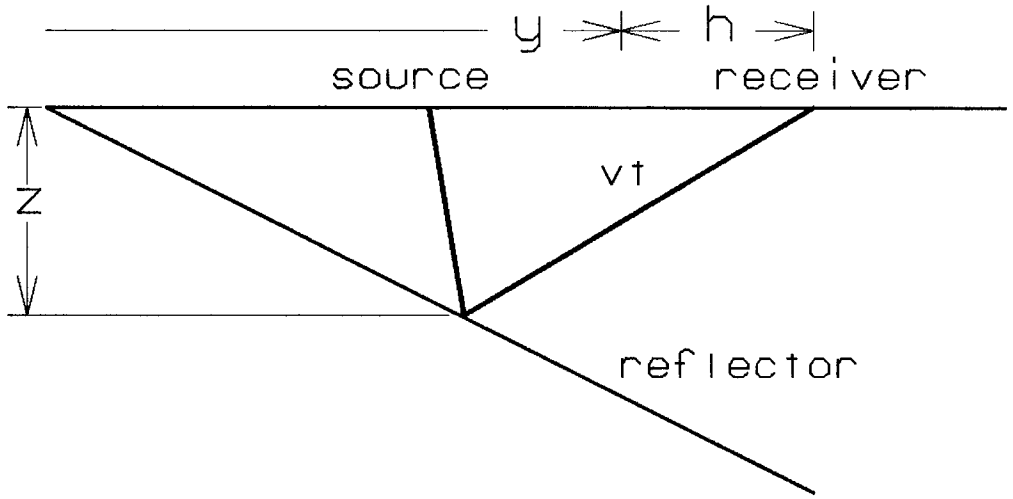

FIGURE 2.5: Geometry of reflection seismology. Lateral coordinates are y for source-receiver midpoint, and h for half offset. Depth is z and time is t.

surface of the earth. An equation to downward continue these traveltimes into the earth is of the form

$$\frac{\partial P}{\partial z} = \Phi \frac{\partial P}{\partial t} \tag{2.7}$$

The expression Φ contains the geometry of the sources and receivers. For a horizontal plane wave Φ is inverse velocity. For a set of sources and receivers everywhere on the surface of the earth along a straight line equation (2.7) becomes

$$\frac{\partial P}{\partial z} = -i\frac{\omega}{v}\left[\sqrt{1-(Y+H)^2} + \sqrt{1-(Y-H)^2}\right] P \tag{2.8}$$

Equation (2.8) is derived in appendix E. This equation has been Fourier transformed over midpoint y, offset h, and time t. These dimensions are shown in Figure 2.5. Basically, one of the square roots is due to the sources and the other due to the receivers.

To make the notation more compact, the terms Y and H represent the ratios

$$Y = \frac{vk_y}{2\omega} \qquad H = \frac{vk_h}{2\omega} \tag{2.9}$$

These ratios have simple interpretations in terms of seismic data and earth angles. Y

is the slope of data on a midpoint section and H is the slope on a CMP gather. In the earth Y is approximately the reflector dip and H is approximately the offset angle.

Common midpoint slant stacks are an obvious way to implement equation (2.8). They directly decompose the seismic data into portions of fixed H. A migration equation is obtained by substituting the formula for slant stacking (2.6) into equation (2.8).

$$\boxed{\frac{\partial P}{\partial z} = -i\frac{\omega}{v}\left[\sqrt{1-(Y+pv)^2}+\sqrt{1-(Y-pv)^2}\right]P} \qquad (2.10)$$

We have made no assumptions about dip, offset, or vertical velocity variations in deriving this formula, so it is exact for migrating seismic data. This formula is computationally nice because a continuous variable k_h has been replaced by a parameter p, thereby reducing the dimensionality of the equation from three to two. This equation operates on midpoint sections (y vs. t) composed of a slant stack constructed from every CMP gather for a fixed ray parameter p. A computer implementation of the solution to this equation is described in appendix G.

2.5. Lateral Velocity Variations

The migration of common midpoint slant stacks was not designed for lateral velocity variations. However, there is strong reason to believe that the effect of lateral velocity variations on slant stacks is not as severe as for conventional stacking. Conventional stacking also does not take into account lateral velocity variations. It sums information across the entire cable length. This leads to imaging and velocity estimation errors (Lynn and Claerbout, 1982). The effective offset width of a slant stack is usually just a fraction of a cable length. This width is approximately that of a Fresnel zone as shown in Figure 2.6.

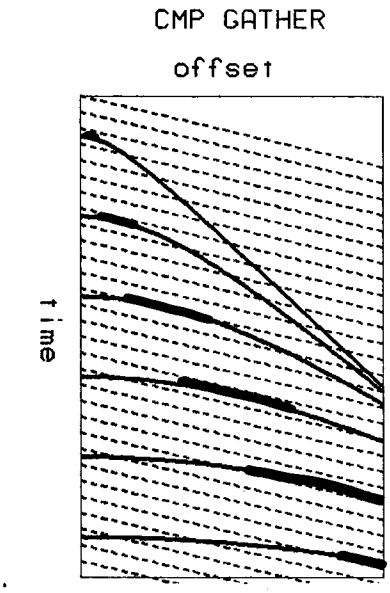

FIGURE 2.6: Effective offset width of slant stacking. A slant stack selects data from a CMP gather at the offsets where the linear stacking trajectory is tangent to the data. The width of offsets contributing to the slant stacking is approximately that of a Fresnel zone. The bounds of the Fresnel zone are the offsets on both sides of the tangency point where the reflection pulse is shifted at least a half cycle at the dominant frequency.

The migration equation (2.10) must be modified in order to handle lateral velocity variations. The lateral wavenumber, k_y in Y, is a composite of every space location. In order to track lateral variations, it must be localized. This is done by inverse Fourier transforming the wavenumber k_y into its space equivalent $i\partial_y$. Claerbout (1976) and Jacobs (1982) describe methods of implementing space domain migration methods.

2.6. Velocity Analysis

The principle of slant stack velocity analysis is the same as for conventional processing: velocity is a function of moveout with offset. However, on a slant stack offset has been transformed into ray parameter. Then velocity becomes a function of moveout with ray parameter.

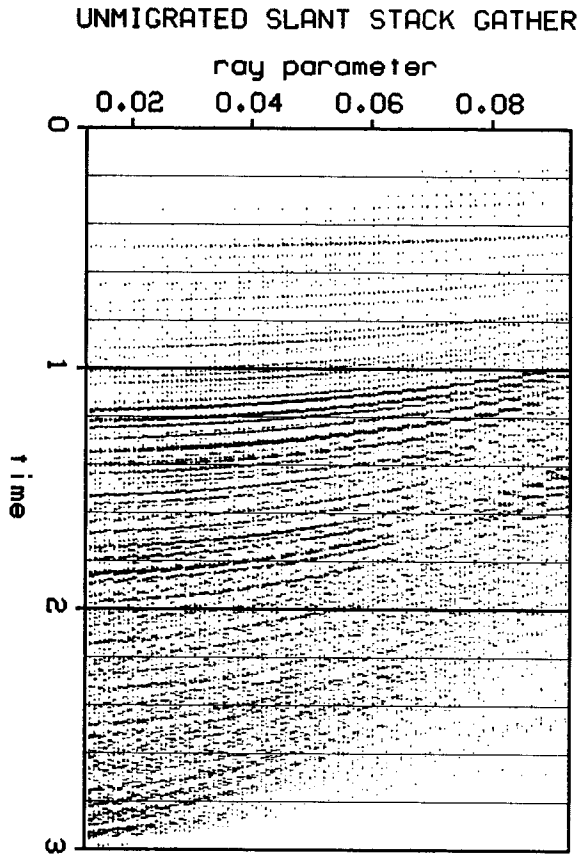

FIGURE 2.7: Unmigrated slant stack gather. Collection of 20 slant stacks, each 5 traces wide, from midpoints 100 to 105 in Figure 2.1. This figure demonstrates how time decreases with increasing ray parameter p. The smallest ray parameter is .015 and the interval is .004 millisecond/feet.

Velocity analysis uses a gather of slant traces made at the same midpoint but for different ray parameters. These are called *slant stack gathers*, an example of which is given in Figure 2.7.

Velocity analysis is performed in a similar manner as is conventional analysis. Moveout paths for various trial velocities as a function of ray parameter are computed using the formulas derived below. These hypothetical moveout paths are matched to actual events on dataset gathers to see which velocity fits best.

Velocity analysis may be done either before or after migration. Migration improves the dataset by moving dipping reflectors to their correct subsurface locations, correcting the distortion of moveout by dip, collapsing diffraction noise, and increasing overall signal to noise.

The situation for estimating velocity after migration is somewhat different than before migration. If the migration is done with the correct velocity, each ray parameter section would appear the same. This implies that migration removes the original moveout present in an unmigrated slant stack gather (Figure 2.8). However,

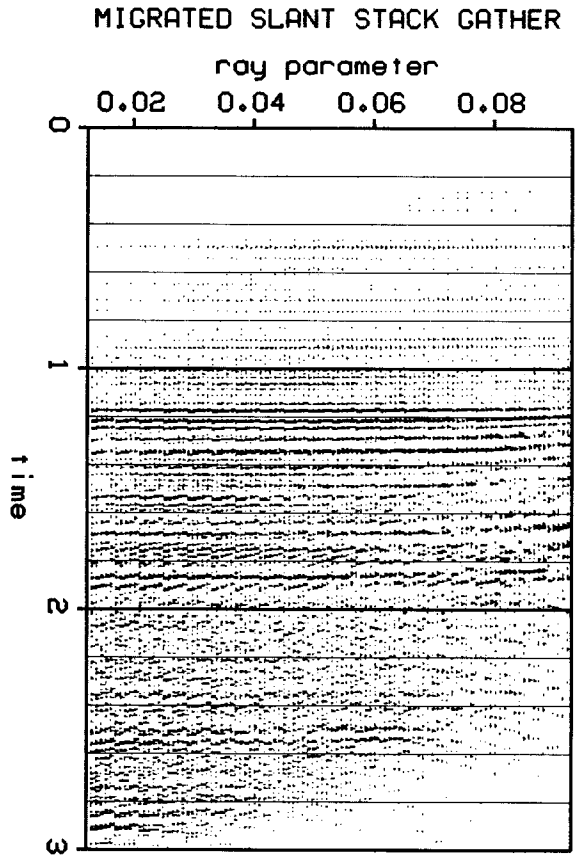

FIGURE 2.8: Migrated slant stack gather. Same slant stack gather as in Figure 2.6, except migrated. Because the migration velocity was nearly correct, the time of a reflector is about the same at any ray parameter.

if the migration velocity is incorrect, then some residual moveout remains. (Figure 2.9) The correct velocity can be determined from this residual moveout.

2.7. Velocity Equation for Unmigrated Gathers

A formula for moveout on a slant stack gather is derived by considering what happens to a reflection hyperbola on a CMP gather that is being slant stacked. Recall the two substages of slant stacking. First, a time shift is applied to each trace, with the amount of the time shift directly proportional to the offset. Then the time shifted trace is summed horizontally across offset.

Start with the equation of a CMP reflection hyperbola

$$t = \left(t_0^2 + \frac{4h^2}{v^2} \right)^{1/2} \tag{2.11}$$

where t_0 is zero offset time and t is time at half-offset h. Then apply a time shift to each seismic trace which is proportional to offset

$$t' = t - 2ph \tag{2.1}$$

The time shifted CMP hyperbola is

$$t' = \left(t_0^2 + \frac{4h^2}{v^2} \right)^{1/2} - 2ph \tag{2.12}$$

Next, sum horizontally across the time shifted hyperbola. The sum is strongest at the apex of the hyperbola. The apex is found by solving for the zero of dt'/dh in equation (2.12) to obtain

$$t' = t_0(1 - p^2v^2)^{1/2} \tag{2.13}$$

The time t' is the slant stack time.

Snell's law is invoked to generalize equation (2.13) to depth velocity variations. Snell's law says that p is invariant with depth in such media, so we just integrate the derivative of equation (2.13) with respect to depth to find t'. Before integrating, we must convert infinitesimals of zero offset time into depth

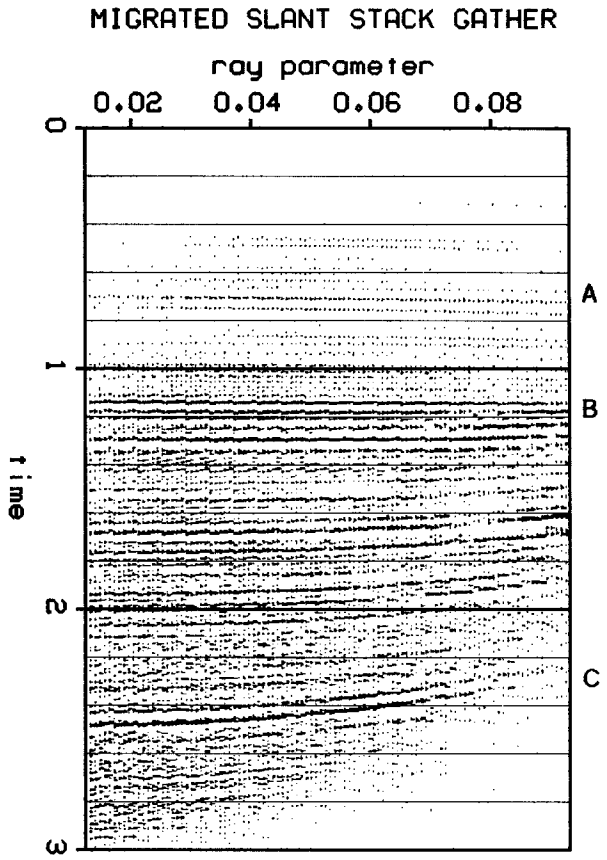

FIGURE 2.9: Slant stack gather migrated with wrong velocity. Same slant stack gather as in Figure 2.6, except migrated with a constant velocity. Because the migration velocity was too high at the top (A) the migration shift was too much, thereby bending reflections downward. Because the migration velocity was too low at the bottom (C) some of the original slant stack time shift which bends upwards, remains.

$$dt_0 = 2\frac{dz}{v(z)} \tag{2.14}$$

Integrating equation (2.13) gives

$$t' = 2\int_0^z \frac{dz}{v}(1 - p^2v^2)^{1/2} \tag{2.15}$$

This equation is used to predict moveout paths for velocity estimation on slant stack gathers. It correctly predicts that the slant stack time of a reflection decreases as

the ray parameter increases (Figure 2.7).

2.8. Velocity Equation for Migrated Gathers

A formula for estimating velocity from migrated slant stacks comes from understanding how migration changes time on a slant stack. It turns out that if the migration was done with the correct depth velocity function then all slant stack traces are converted into zero offset traces. However, if a wrong migration velocity function is used, then the times will differ as a function of the ray parameter p and the correct velocity.

In order to determine how migration changes the time of a slant stack, we begin with the equation for migrating slant stacks

$$\frac{\partial P}{\partial z} = -i\frac{\omega}{\hat{v}}\left[\sqrt{1-(Y+p\hat{v})^2}+\sqrt{1-(Y-p\hat{v})^2}\right]P \qquad (2.10)$$

where $\hat{v}$ is the migration velocity used. Assuming that migration nullifies dip, then the dip dependent term Y is ignored. Then equation (2.10) is inverse Fourier transformed over time to give the time shifting equation

$$\frac{\partial P}{\partial z} = \left[-\frac{2}{\hat{v}}\sqrt{1-p^2\hat{v}^2}\right]\frac{\partial P}{\partial t} \qquad (2.16)$$

The bracketed term is the time shift. The total migration time change is given by integrating this expression over depth.

$$\hat{t} = -2\int_0^z \frac{dz}{\hat{v}}(1-p^2\hat{v}^2)^{1/2} \qquad (2.17)$$

If the migration velocity $\hat{v}$ is the same as the actual velocity v, then the migration time shift $\hat{t}$ is the exact inverse of the original slant stack time shift (t' in equation (2.15)).

The next step is to obtain an equation for time shifts as a function of ray parameter p, migration velocity $\hat{v}$, and actual velocity v. Consider a constant velocity function. Then it can be solved for the unknown true velocity. The slant

stack time shift for an event at depth z with velocity v from equation (2.15) is

$$t' = \frac{z}{v}(1 - p^2 v^2)^{1/2} \tag{2.18}$$

The migration time shift in the other direction puts the reflector at $\hat{z}$.

$$t' = \frac{\hat{z}}{v}(1 - p^2 \hat{v}^2)^{1/2} \tag{2.19}$$

We eliminate variables of the unmigrated gather, t' and z, by solving equations (2.18) and (2.19) together for two different p values.

$$\hat{z}_1 = \left[\frac{(1 - p_1^2 v^2)(1 - p_2^2 \hat{v}^2)}{(1 - p_1^2 \hat{v}^2)(1 - p_2^2 v^2)} \right]^{1/2} \hat{z}_2 \tag{2.20}$$

Equation (2.20) is not as formidable as it seems. It may be interpreted qualitatively by the following chart.

given $p_2 < p_1$:

undermigrated	$\hat{v} < v$	$\hat{z}_1 < \hat{z}_2$	decreasing moveout
exact	$\hat{v} = v$	$\hat{z}_1 = \hat{z}_2$	no moveout
overmigrated	$\hat{v} > v$	$\hat{z}_1 > \hat{z}_2$	increasing moveout

These effects are illustrated in Figure 2.10. It is just an algebraic exercise to solve equation (2.20) for the unknown actual velocity v.

$$v = \left[\frac{\hat{z}_2^2(1 - p_2^2 \hat{v}^2) - \hat{z}_1^2(1 - p_1^2 \hat{v}^2)}{p_2^2 \hat{z}_1^2(1 - p_1^2 \hat{v}^2) - p_1^2 \hat{z}_2^2(1 - p_2^2 \hat{v}^2)} \right]^{1/2} \tag{2.21}$$

Equation (2.21) is used to estimate velocity from two or more measurements of an event on a migrated slant stack gather.

We have not yet found a closed form expression for estimating depth velocity variation. Instead we use equation (2.21) to iteratively estimate thin constant velocity layers in the earth.

2.9. Velocity Estimation from Post-Critical Angle Reflections

Slant stacking manipulates post-critical angle reflections and refractions in a way which is useful for velocity analysis. Waves near the critical angle have the highest amplitudes and are useful on noisy data. McMechan and Ottolini (1980) showed that slant stacking captures these waves in the form of p - τ curves. A p - τ curve (Figure 2.11) is velocity p^{-1} as a single valued function of slant stack time τ (Bessanova et. al., 1976). These curves are also useful for velocity analysis because they express information about velocity gradients between the main reflection interfaces.

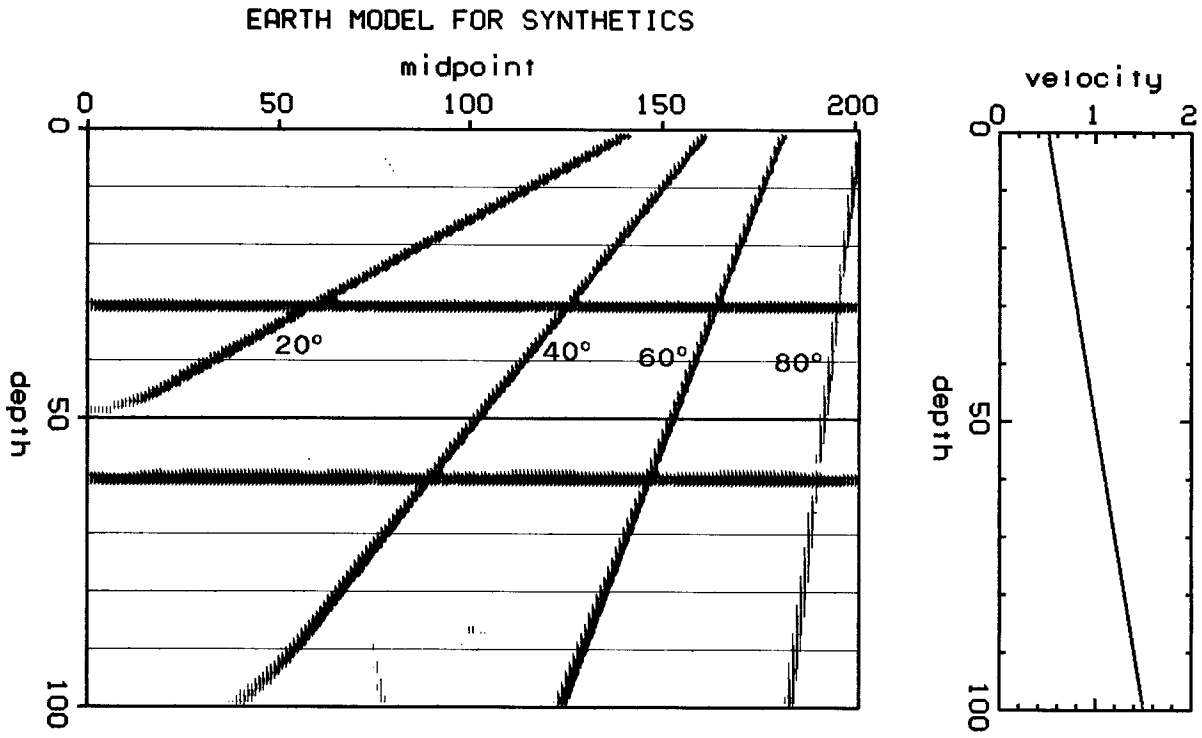

FIGURE 2.10: Earth model for synthetics. This model consists of two flat reflectors and four dipping reflectors up to 80 degrees. The velocity increases linearly with depth. More details of the model are given in appendix A.

Clayton and McMechan (1981) showed that the p - τ curve could be converted to a function of depth using the extrapolation equation (2.16). This method can be extended to dipping reflectors by using equation (2.10) instead of equation (2.16). As with pre-critical reflections, unmigrated dipping reflectors distort the p - τ curve by being at wrong sub-surface locations and give a false high velocity. Figure 2.11 shows that slant stack migration improves p - τ curves of dipping reflectors.

2.10. Synthetic Results

Images from the slant stack migrations of the synthetic of Figure 2.9 are shown in Figure 2.12 to 2.14. This model was a rather severe case of steep dips, wide offsets, and depth velocity variation. The migrations worked rather well compared to conventional processing.

2.11. Conclusions

Migrating common midpoint slant stacks alleviates the steep dip and dip selectivity problems present in migration of conventional stacks. This method also appears to increase lateral resolution. Slant stack migration can estimate velocity after migration when the dataset more truly looks like the earth's sub-surface. Slant stack migration can also estimate velocity from wide angle reflections and refractions.

Slant stack migration works well when several conditions are satisfied:

(1) Lateral velocity variations are small within the width of a Fresnel zone.

(2) The receiver arrays have not attenuated the reflections from steep reflectors. This may be checked by observing constant offset sections and high velocity conventional stacks.

(3) Care is taken during the construction of slant stacks.

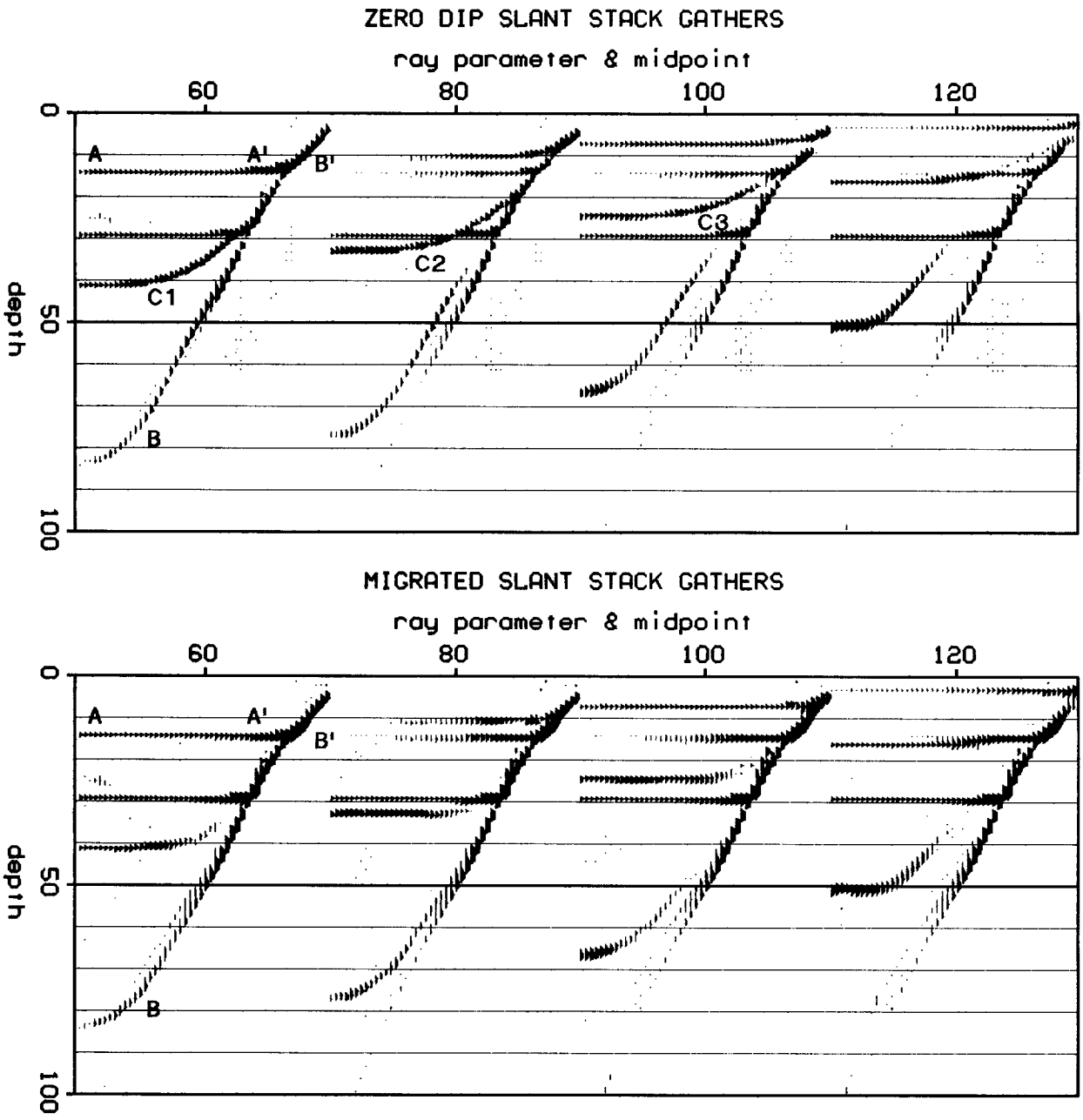

FIGURE 2.11: p-τ migration for dipping reflectors. These are migrated slant stack gathers. The numbers on the horizontal axis are the midpoint from which these gathers were selected on Figure 2.10. Ray parameters increment by .036. These slant stack gathers include both pre-critical and post-critical angle reflections. The pre-critical angle reflections are the horizontal lines (A-A'), behaving the same as in Figure 2.8. The bounding curve (B-B') also called the p-τ curve, comes from the post critical angle reflections. The top gathers were migrated according to the zero dip method of Clayton and McMechan (1981). Dipping reflectors (C1-4) are imaged incorrectly. The bottom shows the same gathers migrated correctly using the method of this thesis.

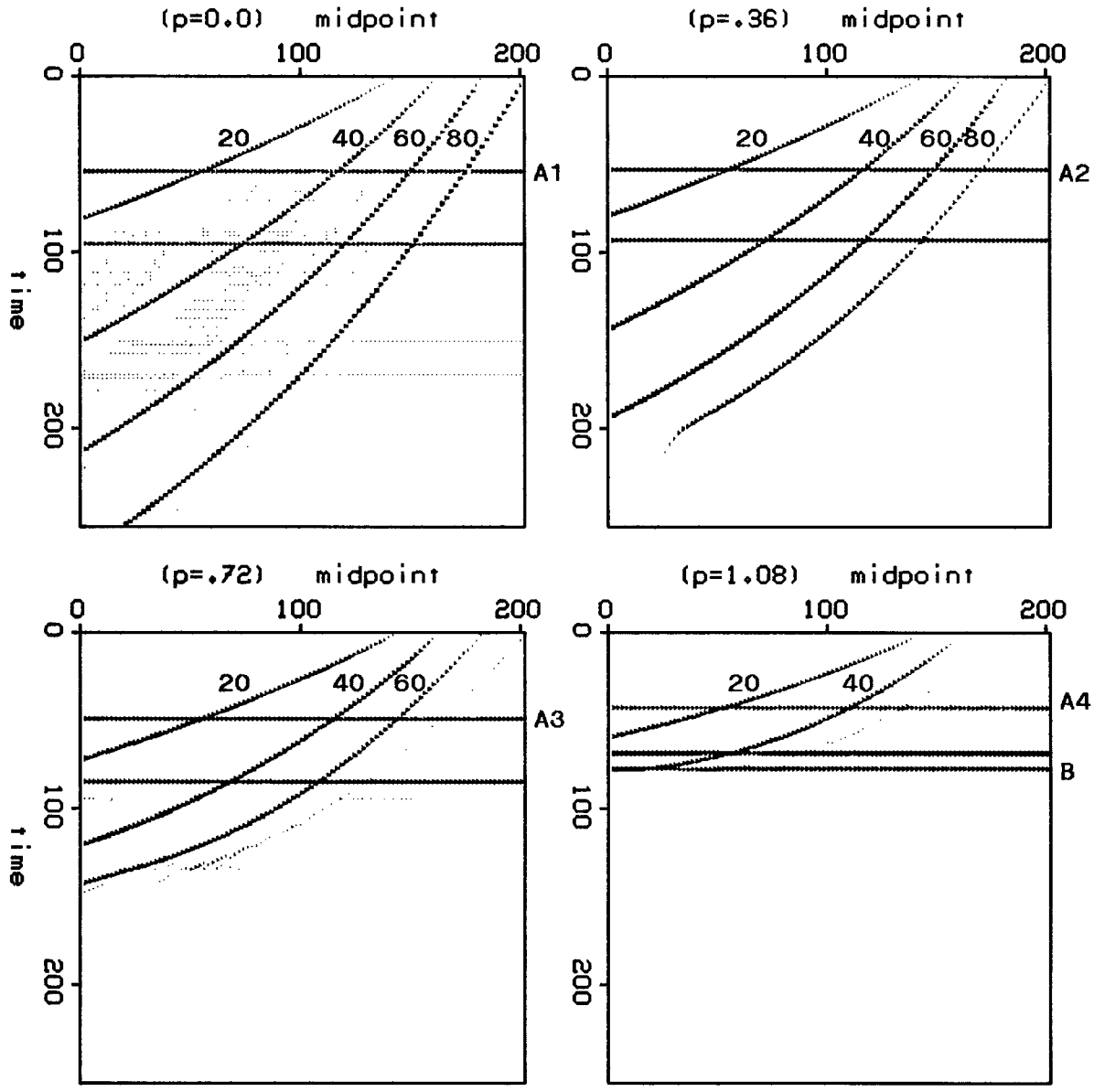

FIGURE 2.12: Synthetic slant stack sections. These unmigrated slant stack sections are made from the linearly increasing depth velocity model of Figure 2.10. The ray parameter is given above each section. The purpose of this model is to test slant stack migration at very steep dips (80°) and relatively wide offsets. Notice the decreasing time moveout (A1-A4) as the ray parameter increases. The steep dipping events (60° and 80°) do not have very steep slopes on a common midpoint gather (appendix figure A.4). Therefore they are not captured on the higher ray parameter sections. The extra line on the last panel (B) is a slant stacking truncation artifact.

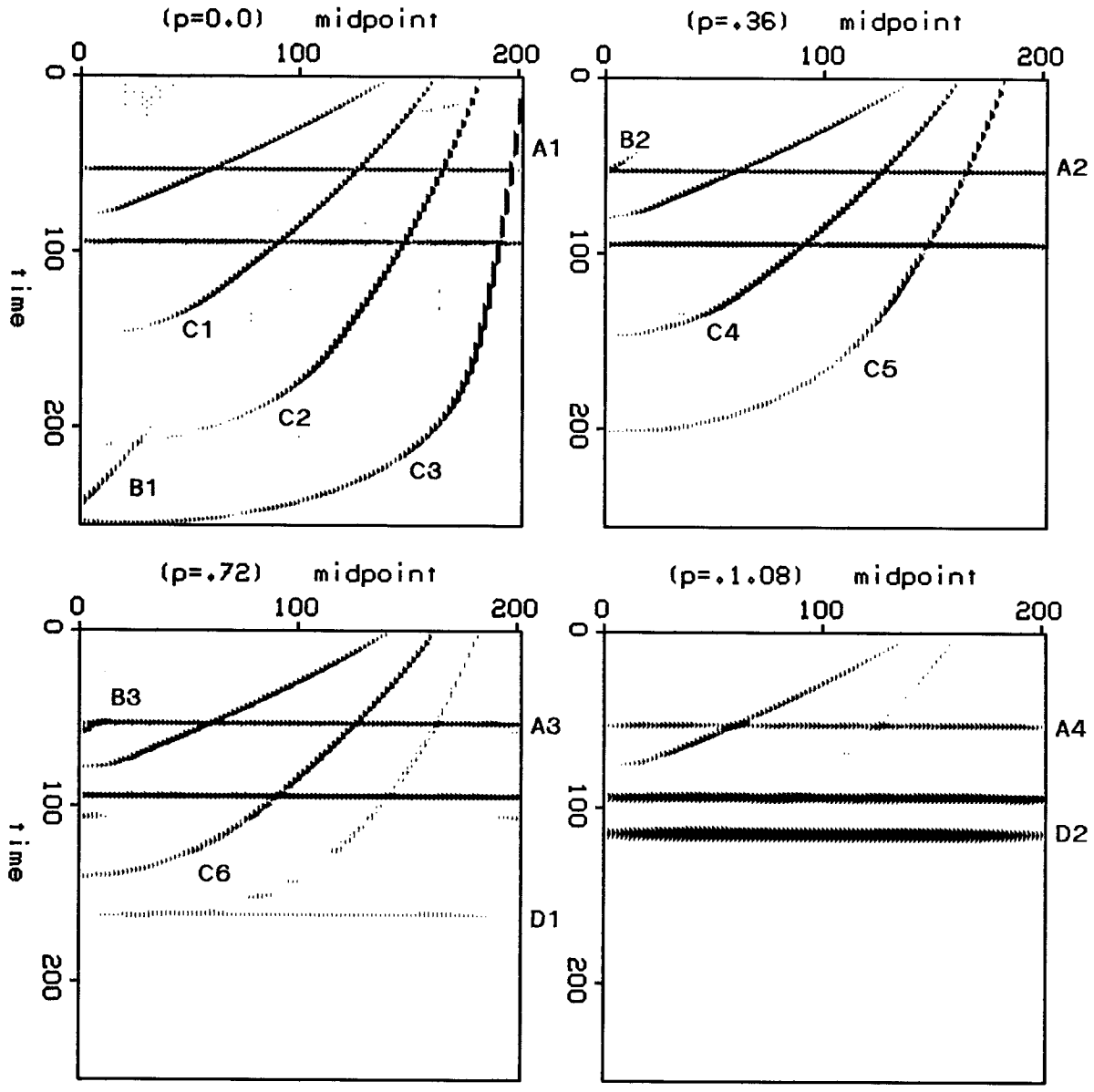

FIGURE 2.13: Migrated synthetic slant stacks. Time migrations of the slant stack panels from the previous figure. These have not yet been converted to depth. Migration converts each panel into an earth image. Therefore migration removes time shifts from the unmigrated panels (A1-4). The curved lines are frequency domain wraparound (B1-3) and reflector truncation tails (C1-6). These are artifacts due to the computer implementation and not the slant stack migration itself. These would go away with a more sophisticated implementation (absorbing sides, etc.). Lines (D1-2) are slant stack truncation artifacts. Since most of these artifacts appear at different places for different ray parameters, they tend to disappear when the sections are stacked together as in the Figure 2.14. The principle that each migrated section is an earth image means that the valid reflections appear in the same place in each section. Therefore they will be reinforced after stacking the sections together.

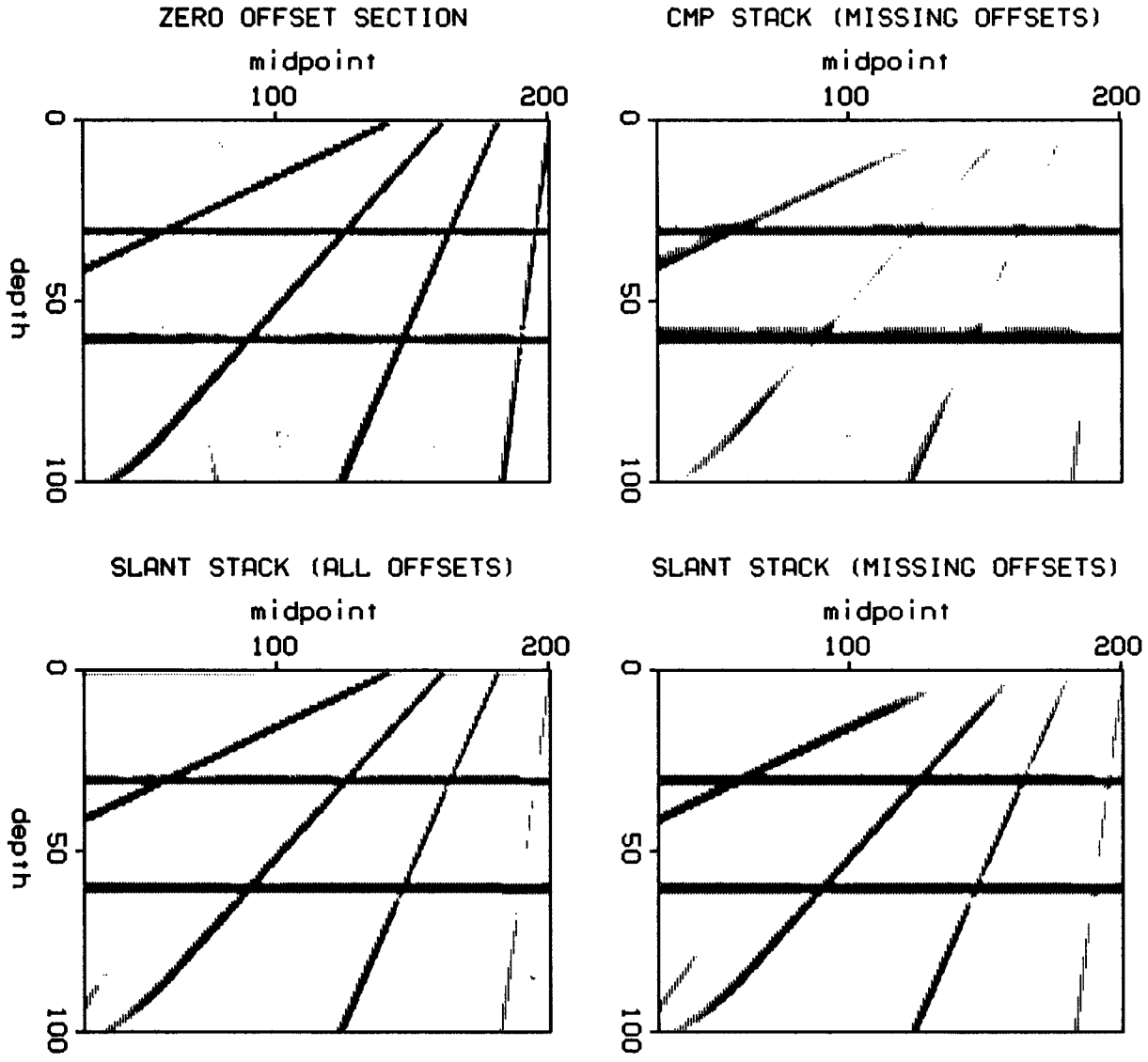

FIGURE 2.14: Migration comparisons. The top left is the migration of the zero offset section, the best possible migration that can be obtain from the data. However, when near offsets are missing, as on the real world, a migration of a conventional stack produces the result in the top right. The lower left is the sum of 50 migrated slant stack sections (Δp=.036). The upper right is the same slant stack migration, except near and wide offsets are missing from the CMP gathers (offsets 10 to 40 retained). Both results are comparable to the zero offset section migration and much better than the conventional stack migration. The missing tops on the two right sections are due to missing inner offsets.